AIAA-2003-3464

Computation of Shock Induced Separated Flow with a Lagged k-ω Turbulence Model

Q. Xiao and H. M. Tsai
Temasek Laboratories
National University of Singapore
Singapore 119260

F. Liu
Department of Mechanical and Aerospace Engineering
University of California, Irvine
Irvine, CA 92697-3975

33rd AIAA Fluid Dynamics Conference
23–26 June 2003
Orlando, FL

Computation of Shock Induced Separated Flow with a Lagged k-ω Turbulence Model

Q. Xiao*, H.M. Tsai†
Temasek Laboratories, National University of Singapore
Kent Ridge Crescent, SINGAPORE 119260

F. Liu+
Department of Mechanical and Aerospace Engineering
University of California, Irvine, CA 92697-3975

ABSTRACT

The lag model proposed by Olsen and Coakley[1] is incorporated into the baseline two-equation k-ω turbulence model to simulate the transonic and supersonic turbulent separated flow. The performances of the lagged k-ω turbulence model is assessed by computing two transonic airfoil flow cases, the RAE2822 Case 10 and the 18% thick double circular arc airfoil, and a separated nozzle flow. The computational results show that for the flow cases with strong separation, the implementation of the lag model improves the results; while for the attached flow cases, the influence of the lag model is not significant.

1. INTRODUCTION

The computation of turbulent separated flow is a challenge for current one and two-equation turbulence models. The difficulty is the inability to account directly for non-equilibrium effects such as those encountered in large pressure gradients involving separation and shockwaves. A new class of model was proposed by Olsen & Coakley[1], which is termed the lag model. The basic idea of the lag model is to take a baseline two-equation model and couple it with a third (lag) equation to model the non-equilibrium effects for the eddy viscosity.

Recently, Xiao et al.[2] incorporated the lag model with the baseline k-ω model and computed the steady/unsteady transonic nozzle flow. Their computations show notable improvements for strong shock cases, with strong non-equilibrium effect present. The computational results with the lag model have shown that the separation predictions are as good or better than those predicted by the Spalart-Almaras or SST models. The lagged k-ω model also enjoys the advantage of not requiring specification of wall distance, and has similar or reduced computational effort compared with Reynolds stress models.

The aim of the present work is to examine the performance of the lag method for transonic and supersonic separated flows. The lag model is here incorporated into the flow code developed by Liu and Ji[3] for solving the coupled Navier-Stokes equations and the k-ω two-equation turbulence model equations by a fully implicit time–accurate multigrid method. Three test cases, i.e.: a steady transonic flow over the RAE 2822 airfoil, a steady and unsteady transonic flow over an 18% thick biconvex circular-arc airfoil, and a separated nozzle flow are investigated. The present study complements our previous studies that indicate significant improvements for steady and unsteady separated flows in a transonic nozzle.

In the following sections, the mathematical model and the numerical solution of these models are outlined. This is followed by the discussion of the numerical results. The conclusions will be made in the final section.

2. MATHEMATICAL MODELING AND NUMERICAL METHODS FOR SIMULATION

The governing equations for the unsteady compressible turbulent flow with the two-equation k-ω and lag model are expressed as follows:

---

*Research Scientist, Temasek Laboratories, National University of Singapore.
†Principal Research Scientist, Temasek Laboratories, National University of Singapore, Member AIAA.
+Associate Professor, Department of Mechanical and Aerospace Engineering, Senior Member AIAA.

Mass conservation:

$$\frac{\partial \rho}{\partial t} + \frac{\partial}{\partial x_j}(\rho u_j) = 0 \tag{1}$$

Momentum conservation:

$$\frac{\partial}{\partial t}(\rho u_i) + \frac{\partial}{\partial x_j}(\rho u_j u_i) = -\frac{\partial p}{\partial x_i} + \frac{\partial \hat{\tau}_{ji}}{\partial x_j} \tag{2}$$

Mean energy conservation:

$$\frac{\partial}{\partial t}(\rho E) + \frac{\partial}{\partial x_j}(\rho u_j H) = \frac{\partial}{\partial x_j}\left[u_i \hat{\tau}_{ij} + (\mu + \sigma^* \mu_T)\frac{\partial k}{\partial x_j} - q_j \right] \tag{3}$$

Turbulent mixing energy:

$$\frac{\partial}{\partial t}(\rho k) + \frac{\partial}{\partial x_j}(\rho u_j k) = \tau_{ij}\frac{\partial u_i}{\partial x_j} - \beta^* \rho \omega k + \frac{\partial}{\partial x_j}\left[(\mu + \sigma^* \mu_T)\frac{\partial k}{\partial x_j} \right] \tag{4}$$

Specific dissipation rate:

$$\frac{\partial}{\partial t}(\rho \omega) + \frac{\partial}{\partial x_j}(\rho u_j \omega) = (\varepsilon \omega / k)\tau_{ij}\frac{\partial u_i}{\partial x_j} - \beta \rho \omega^2 + \frac{\partial}{\partial x_j}\left[(\mu + \sigma \mu_T)\frac{\partial \omega}{\partial x_j} \right] \tag{5}$$

Turbulent eddy viscosity:

$$\frac{\partial}{\partial t}(\rho \nu_t) + \frac{\partial}{\partial x_j}(\rho u_j \nu_t) = a(R_T)\omega \rho (\nu_{tE} - \nu_t) \tag{6}$$

where t is time, x_i position vector, ρ is the density, u_i velocity vector, p pressure, μ dynamic molecular viscosity, ν_{tE} kinematic equilibrium turbulent eddy viscosity, k turbulent mixing energy, and ω the specific dissipation rate. The total energy and enthalpy are $E = e + k + u_i u_i / 2$ and $H = h + k + u_i u_i / 2$, respectively, with $h = e + p/\rho$ and $e = p/[(\gamma - 1)\rho]$. The term γ is the ratio of specific heats. Other quantities are defined in the following equations:

$$\mu_T = \rho \nu_t \tag{7}$$

$$\nu_{tE} = \varepsilon^* k / \omega \tag{8}$$

$$R_T = \rho k / \mu_T \omega \tag{9}$$

$$S_{ij} = \frac{1}{2}\left(\frac{\partial u_i}{\partial x_j} + \frac{\partial u_j}{\partial x_i}\right) \tag{10}$$

$$\tau_{ij} = 2\mu_T\left(S_{ij} - \frac{1}{3}\frac{\partial u_k}{\partial x_k}\delta_{ij}\right) - \frac{2}{3}\rho k \delta_{ij} \tag{11}$$

$$\hat{\tau}_{ij} = 2\mu\left(S_{ij} - \frac{1}{3}\frac{\partial u_k}{\partial x_k}\delta_{ij}\right) + \tau_{ij} \tag{12}$$

$$q_j = -\left(\frac{\mu}{\mathrm{Pr}_L} + \frac{\mu_T}{\mathrm{Pr}_T}\right)\frac{\partial h}{\partial x_j} \tag{13}$$

$$a(R_T) = a_0\left[\frac{(R_T + R_{T0})}{(R_T + R_{T\infty})}\right] \tag{14}$$

Where Pr_L and Pr_T are the laminar and turbulent Prandtl numbers, respectively. The other coefficients are:

$a_0 = 0.35$, $R_{T0} = 1$, $R_{T\infty} = 0.01$, $\varepsilon = 5/9$, $\varepsilon^* = 1$, $\beta = 0.075$, $\beta^* = 0.09$, $\sigma = 0.5$, $\sigma^* = 0.5$.

It is known that, conventional one- and two-equation turbulence models generate Reynolds stresses that respond too rapidly to changes in mean flow conditions partially due to the need to accurately reproduce equilibrium flows. Therefore, these baseline turbulence models give unsatisfactory results for flows with significant separation under adverse pressure gradients or across shock waves. In the above formulation Eqns (1-6), the standard k-ω turbulent model is kept unchanged. However, the k and ω are only used to predict the 'equilibrium' eddy viscosity ν_{tE}. An additional equation, Eqn. (6), is used to predict the actual eddy viscosity ν_t. This lag equation is essentially a relaxation model intended to account for memory effects of the turbulence eddy viscosity in adjusting to its local equilibrium value. On the other hand, it is shown by Olsen and Coakley[1] that Eqn. (6) is decoupled from the k and ω equations for such equilibrium turbulence flows as the decay of isotropic homogeneous turbulence and fully developed channel flows.

The basic numerical method used to solve the above system of equations in this paper follows that described in detail by Liu and Ji[3]. The integral forms of the conservation equations are discretized on quadrilateral cells using the finite volume approach. A staggered scheme is used for the coupling of Navier-Stokes equations, the k-ω and lag equations. A central difference scheme is used to discretize the diffusive terms and an upwind Roe's scheme is used for convective terms in the Navier-Stokes and the k-ω equations.

For the lag model, the spatial discretization is the same as the k-ω model. The source term at the right-hand

side of the lag equation is a nonlinear term, the explicit time marching formula for the k, ω and υ_t equations within each stage of a multistage time-stepping scheme is modified to treat the source terms implicitly. (Liu and Ji[3])

$$(\rho\nu_t)^{n+1} - (\rho\nu_t)^n = \frac{-R_\nu^n \Delta t}{1 + a\omega\Delta t} \tag{15}$$

where R_ν^n is the residual for the ν_t equation at time step n.

The ρk, $\rho\omega$ and $\rho\nu_t$ equation are solved simultaneously. The non-equilibrium eddy viscosity $\rho\nu_t$ is updated after each stage of time step.

After being discretized in space, the governing equations are reduced to a set of ordinary differential equations with only derivatives in time.

$$\frac{d}{dt}(\vec{W}_{ij}V_{ij}) + \vec{R}(\vec{W}_{ij}) = 0 \tag{16}$$

where $\vec{W} = [\rho, \rho u_i, \rho E, \rho k, \rho\omega, \rho\upsilon_t]^T$, V_{ij} is the volume of the i, j cell and $\vec{R}(\vec{W}_{ij})$ is the residual which is obtained by evaluating the flux integral in Eqns (1-6).

The dual time stepping method proposed by Jameson[5] is adopted here for the time discretization. The method uses an implicit physical time discretization. At each physical time step, the equations are integrated in a pseudo-time to obtain the solution to the steady state in pseudo-time.

To obtain a fully-implicit algorithm, Eqn. (16) is approximated as follows:

$$\frac{d}{dt}(\vec{W}_{ij}^{n+1}V_{ij}^{n+1}) + \vec{R}(\vec{W}_{ij}^{n+1}) = 0 \tag{17}$$

where the superscript n+1 denotes the time level (n+1)Δt. The $\frac{d}{dt}$ operator is approximated by an implicit backward difference formula. For a second-order accurate operator, Eqn. (17) can be expressed in the following form:

$$\frac{3}{2\Delta t}\left[\vec{W}_{ij}^{n+1}V^{n+1}\right] - \frac{2}{\Delta t}\left[\vec{W}_{ij}^{n}V^{n}\right] + \frac{1}{2\Delta t}\left[\vec{W}_{ij}^{n-1}V^{n-1}\right] + \vec{R}(\vec{W}_{ij}^{n+1}) = 0 \tag{18}$$

Eqn. (18) represents an implicit set of coupled ordinary differential equations. These equations can be solved at each time step using the same multistage technique for explicit steady-state calculations if we define the modified residual $\vec{R}^*(\vec{W})$ as

$$\vec{R}^*(\vec{W}) = \vec{R}(\vec{W}) + (3/2\Delta t)(\vec{W}V^{n+1}) - (2/\Delta t)(\vec{W}^n V^n) + (1/2\Delta t)(\vec{W}^{n-1}V^{n-1}) \tag{19}$$

and march to steady-state in a fictitious time t^* with the following system of ordinary differential equations:

$$\frac{d\vec{W}}{dt^*} + \vec{R}^*(\vec{W}) = 0 \tag{20}$$

Within each real time step, the set of ordinary differential Equations (20) is solved using a explicit five-stage Runge-Kutta scheme. To accelerate the convergence, unsteady multigrid method proposed by Jameson[4] and further implemented by Liu and Ji[3] is applied in the present study for all equations corresponding to Eqns (1)-(6) in a coupled fashion.

3. RESULTS AND DISCUSSIONS

The numerical method presented above is applied to three sets of problems namely the steady transonic flow over the RAE2822 airfoil (Cook et al.[5], Kral[6], Haase et al.[7] Haase[8] and Thomas et al.[9]), steady/unsteady flow over an 18% thick circular-arc airfoil (McDevitt et al.[10], Levy[11] and Rumsey et al.[12]), and a separated nozzle flow (Hunter[13]). The results are presented and discussed below.

3.1 Steady Transonic flow over RAE2822

Since the main purpose of the present study is to investigate the effect of the lag model on shock induced separation, only the test case denoted as Case 10 by Cook et al.[5] is used. Cook et al.[5] reported that the shock in Case 10 is sufficiently strong to induce flow separation after the shock. The experimental flow parameters obtained in the wind tunnel are: Ma=0.75, Re=6.2x10^6, α=3.19°. Turbulent transition in the experiments is induced by tripping the flow near the leading edge of the airfoil at x/c=0.03 on both the upper and lower surfaces of the airfoil. To compare the experimental data with the computed flow around the airfoil in free-flight conditions, corrections to the tunnel data are suggested (Kral[6], Haase et. al.[7], Haase[8] and Thomas et. al.[9]). The flow conditions used in the current computations adopt those as used in the EUROVAL project (Haase et. al.[7]). For Case 10, Ma=0.754, Re=6.2x10^6, α=2.57°.

The mesh for the present computation is a C-mesh, which extends 20 chord lengths in all directions. The mesh consists of 384x64 cells with 256 cells on the airfoil surface. The average y+ value of the first cell above the wall is less than 1.

Fig.1 shows the typical convergence history for mass, ρk, $\rho\omega$ and $\rho\upsilon_t$ for the RAE2822 Case 10 using 3 multigrid levels and a CFL number of 8. Within 500 multigrid cycles, the residual of ρk, $\rho\omega$ and $\rho\upsilon_t$ equation is reduced by two to three magnitudes while the residual of mass equation is reduces by 4-5 orders.

The comparison of computed pressure coefficient, Cp, with experimental data is shown in Fig. 2. Neither of computations with or without inclusion of the lag model is able to accurately predict the shock location. The predicted shock location is too far downstream compared to the experimental data.

Fig. 3 shows the comparison of the calculated skin friction coefficient, Cf, distribution with experimental data. It is noted that the skin friction on the pressure side of the airfoil predicted by the baseline k-ω model is almost the same as that predicted by the lag model. On the upstream side of the airfoil, the skin friction predicted by the lag model is slightly smaller than that by the baseline model. Both results with and without the lag model predict similar sizes of the separated flow zone, which starts downstream from the shock and reattaches at the rear of the airfoil.

The predictions of the lift and drag coefficients Cl and Cd are listed in Table 1 along with experimental data. The drag and lift predictions with the lag model are better than without the lag model but comparatively cannot be considered as significant improvements.

Fig. 4(a)-(f) show the velocity profiles at six different stream-wise locations. The computational results agree well with the experiments except in the region of adverse pressure gradient (x/c=0.574, 0.65 and 0.75). Larger differences can be observed at x/c=0.574 which reflects the differences in the computed shock location. The positions x/c=0.65 and 0.75 lie downstream of the shock and flow separation occurs at x/c=0.65. The results in Fig.4(c) show that the flow after the separation is not well predicted. The prediction with the lag model at x/c=0.65, yields a slight improvement compared to the results without the lag model. The lag model has only a small influence on the velocity profile, which is not unexpected since the separation point and shock location differs from the experimental data.

The RAE2822 Case 10 has been extensively used for validation of Navier-Stokes codes applied to transonic airfoil flow, since it is being more sensitive with respect to different turbulence model applied (Kral[6], Haase et al.[7], Haase[8] and Thomas et al.[9]).

In the comparative study of Kral[6], several different turbulence models such as: the Baldwin-Lomax algebraic model, the Spalart-Allmaras one-equation model, four low-Reynolds-number $k-\varepsilon$ two-equation models and Menter's zonal $k-\omega/k-\varepsilon$ two-equation models are used. The investigation of Haase[8] employed the Cebeci-Smith algebraic turbulence model and the Johnson-King, Johnson-Coakley ½-equation model as well as three two-equation models Lien-Leschziner, Chien and Kalitzin $k-\tau$ models. The SST model in the study by Kral[6] gave the best prediction of the shock location and the mean velocity profiles compared to the experiment.

Predictions of Case 10 with two-equation models exhibit similar noticeable trends. They tend to underpredict pressure induced separation or dismiss separation completely. The Johnson-King and Johnson-Coakley ½-equation turbulence model, which take into account the boundary layer history effect by solving an ordinary differential equation, give the best approach when compared to the experiment. In the study of Thomas et al. [9], except for the Baldwin-Lomax algebraic model and the two-equation $k-\varepsilon$ model, an RSM (Reynolds Stress Model) and an RSM-GGDH (Reynolds Stress Model with Generalized Gradient Diffusion Hypothesis) are adopted. Their computations show that none of the turbulence models are able to accurately predict the shock location with all turbulence models predicting a separation region at the foot of the shock. The RSM model gives results that are closest to the experimental values though not in complete agreement.

The deviations from the experiment in the present studies are consistent with predictions by other attempts. One additional point is worthy to be pointed out when comparing the computation with the wind-tunnel experimental results. It is well known that most of the experimental measurements are done in wall-bounded wind tunnel, which is different from the CFD computation with free-flight conditions. To compare the computation with the experimental measurement, the correction on the flow conditions are needed. However, different authors used varied corrections, (Kral[6]: $Ma_\infty = 0.75, \mathrm{Re}_\infty = 6.2x10^6$ and $\alpha = 3.19$; Haase[8]: $Ma_\infty = 0.754, \mathrm{Re}_\infty = 6.2x10^6$ and $\alpha = 2.81$; Thomas et al.[9]: $Ma_\infty = 0.754, \mathrm{Re}_\infty = 6.2x10^6$ and $\alpha = 2.57$). Such

uncertainties add to the variations in the computational results.

3.2 Steady and Unsteady Transonic Flow around 18% thick circular-arc Airfoil

The second test case is the transonic flow over an 18% thick circular-arc airfoil. Previous experimental and numerical studies (McDevitt et al.[10], Levy[11] and Rumsey et al.[12]) have indicated that, the flow over this circular-arc aerofoil exhibit varied behavior depending on the flow conditions. Three distinct regions have been observed for a fixed free-stream Reynolds number but varied Mach number; below a critical Mach number, the flow is steady with trailing edge separation, the flow is characterized by a weak shock wave near the mid-chord with trailing-edge flow separation. For larger Mach number, shock induced separation is encountered and the flow becomes unsteady, with unsteady shock motions on the upper and lower surface that are out of phase with each other. As the Mach number is increased, a steady shock reappears. It is sufficiently strong to induce flow separation. To study the influence of the lag model in this steady/unsteady shock induced oscillation problem, the computation is conducted for a fixed free-stream Reynolds number $\mathrm{Re}_\infty = 10x10^6$ and three different mach numbers: $Ma_\infty = 0.73$, 0.76, and 0.79.

Figs. 5(a) and (b) show the top wall pressure coefficient (Cp) distribution and velocity vectors for $\mathrm{Re}_\infty = 10x10^6$ and $Ma_\infty = 0.73$. Consistent with the experimental findings the computational results reveal that, under these flow conditions, the flow is steady with a weak trailing edge separation as shown in Fig. 5(b). The influence of the lag model is small as shown in Fig.5(a).

At $Ma_\infty = 0.76$, the computation indicates the flow becomes unsteady with shock-induced oscillation. The typical lift coefficient (Cl) variation within one cycle is shown in Fig. 6(a) and a spectral analysis shown in Fig. 6(b) reveals one dominant reduced frequency (0.41). The comparison with and without the lag model reveals that the magnitude and oscillation frequency are more or less identical except some slight difference in the phase angle of Cl. Figs. 7(a) and (b) show the distribution of the time-mean pressure coefficient on the top wall and the movement of the shock location within one cycle along with the experimental data from McDevitt et al.[10]. The different time instances are defined in Fig. 6(a). As seen from both figures, the improvement with the lag model is not very significant for this moderate Mach number.

At $Ma_\infty = 0.79$, the computation shows the flow develops into steady state again. The pressure coefficient distribution (Cp) and skin friction (Cf) distribution with and without the lag model for $Ma_\infty = 0.79$ are shown in Figs. 8(a) and (b), respectively, along with the experimental data. As indicated by both figures, the flow well upstream of the shock ($0<x/c<0.6$) is close to its equilibrium state, therefore, the prediction of the lag and baseline model are identical. However, in the vicinity and downstream of the shock, the prediction with the lag model is significantly better than that with the baseline k-ω model.

To better understand the influence of the lag model, the streamlines of the flow and the contours of the turbulent eddy viscosity μ_t for $\mathrm{Re}_\infty = 10x10^6$ and $Ma_\infty = 0.79$ are plotted in Figs. 9(a) and (b). Fig. 9(a) shows, in the shock and post shock region, shock induced separation occurs. The basic difference between the lag model and baseline model is that the lag model predicts a much smaller turbulent eddy viscosity in the separation region. In fact, Fig. 9(b) indicates that the baseline model predicts μ_t in the range between $8.15x10^{-5}$ and $2.35x10^{-3}$, compared to that between $8.15x10^{-5}$ and $8.15x10^{-4}$ with the lag model. The smaller turbulent viscosity causes less momentum transport from the freestream to the wall, thus increasing the probability for separation, which gives better accounts for the non-equilibrium part of the flow.

3.3 Steady Separated Nozzle Flow

The third problem under investigation is a 2-D planar convergent-divergent separated nozzle flow as experimentally studied by Hunter[13]. The computational domain is shown in Fig.10, which includes the ambient region surrounding the nozzle. Relative to the nozzle exit, it extends 30 throat-heights downstream, 25 throat-heights upstream, and 25 throat-heights normal to the jet axis. The grid used in the computation is 1216x128 with the average first grid point near wall y+ < 1 which is shown in Fig.11. As can be seen from the figure, the grids are clustered near the wall, nozzle throat, and the jet region.

For the inflow at AB we set, $p_t = NPR \times p_a(psia)$, $T_t = T_a$ where p_t is the total pressure, p_a is the static ambient pressure, T_t the total temperature and NPR is Nozzle Pressure Ratio. The inlet value of ω is estimated as: $\omega = \mathrm{O}(10u/h)$ where u is the velocity at the inlet (AB) boundary and h is the height of throat. The turbulent energy k is specified with a small

value to keep the inlet eddy viscosity at low level. For the lag equation the inlet eddy viscosity ν_t is set to ν_{tE}. The inflow boundary condition is specified as $p_a = 14.85(psia)$, $T_a = 530^0 R$. For the outflow condition EF only the pressure is specified as the ambient pressure (p_a) and all the other variables are extrapolated. At the boundary CD, ambient inflow boundary condition is specified ($p_a = 14.85(psia), T_a = 530^\circ$ R). Far-field characteristic boundary condition is specified along DE. while symmetric boundary condition is specified along AF. Zero velocity is imposed and the pressure is extrapolated to the wall at the wall boundaries (BG and CG). Here the turbulent mixing energy k is set to zero. The specific dissipation rate ω must satisfy the following asymptotic solution as the wall is approached:

$$\omega \to \frac{6\nu_w}{\beta y^2} \qquad \text{as the distance } y \to 0$$

In all of our numerical examples, the above equation is enforced only at the first grid point from the wall. The eddy viscosity ν_t is set to its equilibrium value ν_{tE}.

As pointed out by Hunter[13], the flow for NPR≥2.4 can be regarded as a 2-D flow. For NPR≥5.4, the flow in the nozzle becomes shock free. To focus on the lag influence on the shock-induced separated flow, the computational results presented below will focus on cases where NPR is between 2.4 and 5.4.

Figs. 12(a) and (b) show the pressure distributions on the top wall for NPR=2.4 and NPR=3.0, respectively. For comparison, the experimental results of Hunter[13] are also included. Both figures clearly show that the calculation with the lag model accurately predicts the pressure distribution and shock location when compared to the experimental data. The predictions without the lag model incorrectly locate a more downstream shock position.

The Mach contour comparison with and without the lag model are shown in Figs. 13(a) and (b) for NPR=2.4 and NPR=3.0, respectively. It is obvious that, the lambda shock location predicted by the lag model is more upstream than these predicted without the lag model and closer to the experiment.

The streamlines of the flow and the turbulent eddy viscosity contour near the exit part of nozzle are shown in Figs.14 (a) and (b), respectively. As indicated in Fig. 14(a), a separation vortex occurs in the vicinity of the nozzle exit. Like in the previous test cases the turbulent viscosity contour in Fig. 14(b) shows that the prediction with the lag model produces a lower value of μ_t than the baseline model, thus better reflects the physics of separated flow.

4. CONCLUSIONS

A baseline k-ω turbulent model with and without a lag equation model is solved with a multigrid finite-volume method to examine shock induced separated flow. Three flow cases are considered, namely, transonic airfoil RAE2822, 18% thick circular-arc airfoil, and separated nozzle flow. The results are presented and compared with available experimental data. The main conclusions can be summarized as follows:

1) For the RAE2822 airfoil Case 10, which has strong flow separation, the improvement is slight with the inclusion of the lag model. The improvements are comparable to other models that are intended for such use. Like in previous studies the present calculations do not coincide with the experimental data.

2) Computations of the 18% thick circular-arc airfoil shows that, for the case with weak shock-induced separation ($\mathrm{Re}_\infty = 10x10^{-6}$ and $Ma_\infty = 0.73, 0.76$), the influence of the lag model is not as significant. For the strong separation case ($\mathrm{Re}_\infty = 10x10^{-6}$ and $Ma_\infty = 0.79$), the shock location is significantly better predicted. In the unsteady shock induced oscillation studies ($\mathrm{Re}_\infty = 10x10^{-6}$ and $Ma_\infty = 0.79$), the impact of the lag model is small.

3) For separated flow in a nozzle, notable improvement can be observed in using the lag model as the wall pressure distribution indicates. It accurately captures the location of the shock.

In general, with the lag model the computations give better predictions of the flow physics for the strong separated flow cases. However it appears that the lag model does not improve the results as much for external flows than for internal nozzle flows based on the present new results and results from our previous studies of a steady and unsteady nozzle flows (Xiao et al.[2]). It is perhaps due to uncertainties and difficulties for experiments to model external separated flows in a confined wind tunnel. More studies are needed to assess this.

REFERENCES

1. Olsen, M.E. and Coakley, T.J., "The lag model, a turbulence model for non-equilibrium flows," AIAA 2001-2564, 2001.
2. Xiao, Q., Tsai, H.M. and Liu, F., "Computation of transonic diffuser flows by a lagged k-ω turbulence model," to appear in *Journal of Propulsion and Power, vol. 19, no. 3, May-June, 2003.*
3. Liu, F. and Ji, S., "Unsteady flow calculations with a multigrid Navier-Stokes Method," *AIAA Journal*, Vol. 34, No. 10, 1996, pp. 2047-2053.
4. Jameson, A., "Transonic flow calculations," Princeton Univ., Dept. of Mechanical and Aerospace Engineering, MAE Rept. 1651, Princeton, NJ, July, 1983.
5. Cook, P.H., McDonald M.A. and Firmin, M.C.P., "Aerofoil RAE2822-pressure distributions and boundary layer and wake measurements," AGARD AR 138, pp.A6-1 to A6-77.
6. Kral, L.D., "Recent experience with different turbulence models applied to the calculation of flow over aircraft components," *Progress in Aerospace Sciences*, Vol. 34, November, 1998, pp481-541.
7. Haase, W., Brandsma, F., Elsholz, E., Leschziner, M., and Schwamborn, D. "EUROVAL-An European initiative on validation of CFD codes," *Notes on Numerical Fluid Mechanics*, Vol. 42, Vieweg Verlag, 1993, pp. 127-184.
8. Haase, W. "Case studies of applications of turbulence models in aerospace," AGARD report-R-819, 1997.
9. Thomas, H. and Lars, D., "Reynolds stress transport modeling of transonic flow around the RAE2822 airfoil," AIAA 94-0309, 1994.
10. McDevitt, J.B. Levy, L.L. and Deiwert, G.S. "Transonic flow about a thick circular-arc airfoil," *AIAA Journal*, Vol.14, No.5, 1976, pp.606-613
11. Levy L.L. "Experimental and computational steady and unsteady transonic flows about a thick airfoil," *AIAA Journal*, Vol.16, No.6, 1978, pp.564-572.
12. Rumsey, C.L., Sanetrik, M.D., Biedron, R.T., Melson, N.D. and Parlette, E.B. "Efficiency and accuracy of time-accurate turbulent Navier-Stokes computation," *Computers & Fluids*, Vol. 25, No.2, 1996, pp. 217-236.
13. Hunter, C.A., "Experimental, theoretical, and computational investigation of separated nozzle flows," AIAA 98-3107 1998.

	C_L	C_D
Experiment	0.735	0.0239
Without the lag model	0.8102	0.0271
With the lag model	0.7692	0.0258

Table 1 Comparison of drag and lift coefficient with experimental data for RAE2822.

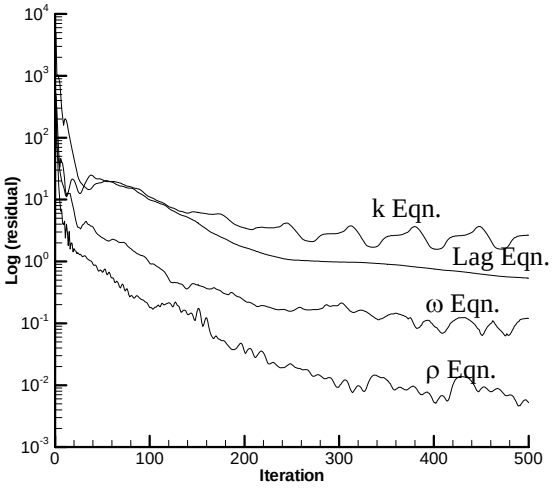

Fig.1 Convergent history for RAE2822, Case 10 transonic flow calculations.

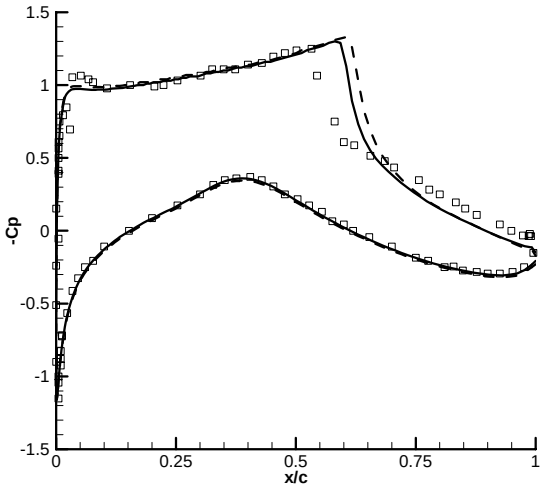

Fig. 2 Pressure coefficient distribution for RAE2822, Case 10. Square: experiment; Dashed line: results without the lag model; Solid line: results with the lag model.

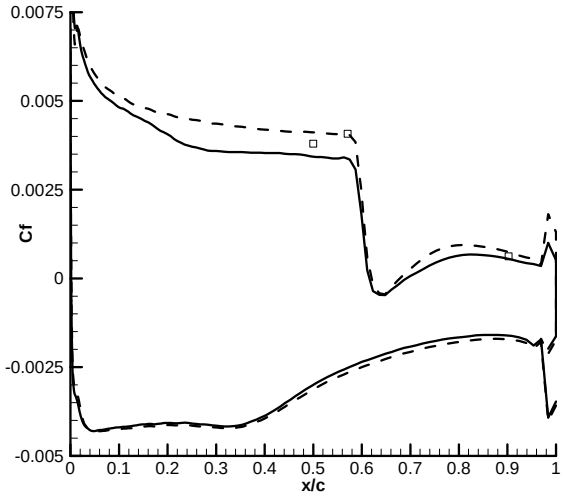

Fig. 3 Skin friction coefficient distribution for RAE2822, Case 10. Square: experiment; Dashed line: results without the lag model; Solid line: results with the lag model.

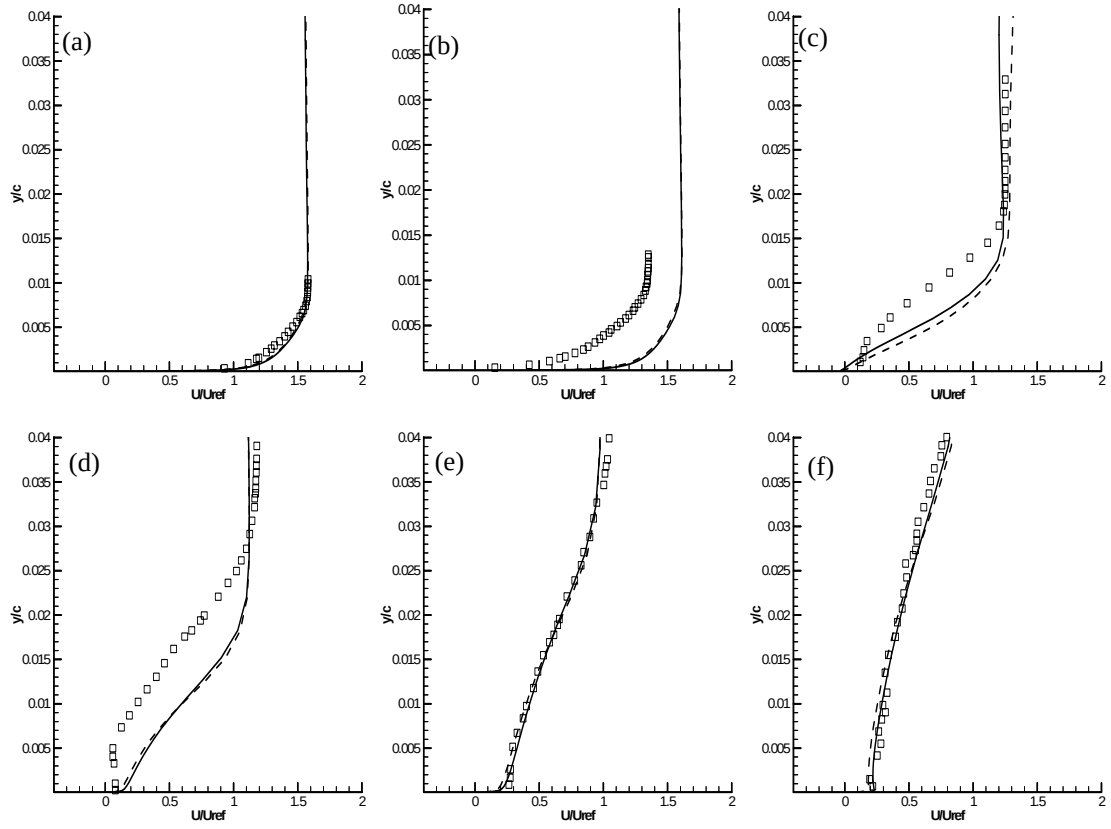

Fig. 4 Velocity profiles at different streanwise locations for RAE2822. Square: experiment; Solid line: with the lag model; Dashed line: without the lag model (a) x/c=0.498, (b) x/c=0.574, (c) x/c=0.65, (d) x/c=0.75, (e) x/c=0.9, (f) x/c=1.0.

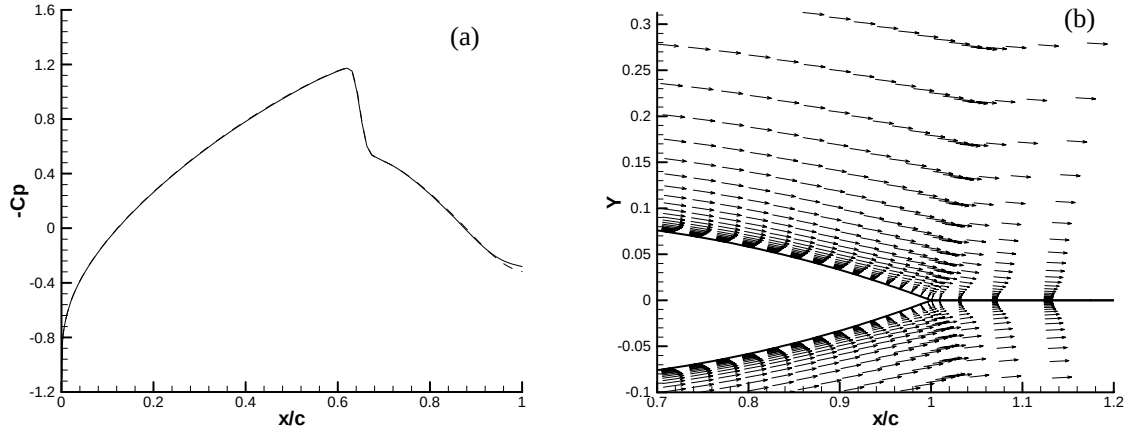

Fig. 5 Top wall pressure coefficient distribution and velocity vectors for transonic flow around 18% thick circular-arc airfoil ($\mathrm{Re}_\infty = 10x10^6, Ma_\infty = 0.73$) (a) Top wall pressure coefficient distribution. Solid line: with the lag model; Dashed line: without the lag model. (b) Velocity vectors (for clarity, the velocity vectors are drawn by skipping 3 grid lines in x direction).

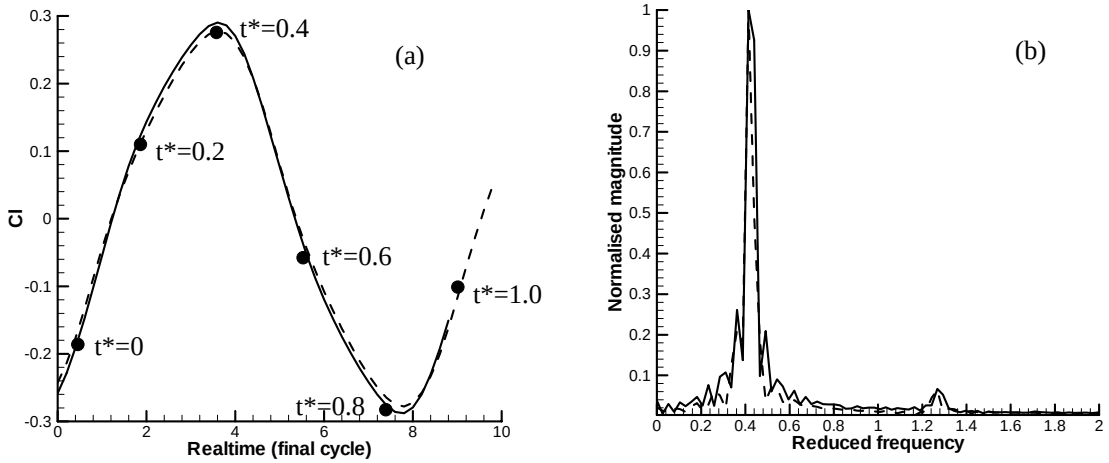

Fig. 6 The lift coefficient variation within one cycle and its Fourier spectrum. (transonic flow around 18% thick circular-arc airfoil $\mathrm{Re}_\infty = 10x10^6, Ma_\infty = 0.76$). (a) Lift coefficient. Solid line: with the lag model; Dashed line: without the lag model. (b) Fourier spectrum. Solid line: with the lag model; Dashed line: without the lag model.

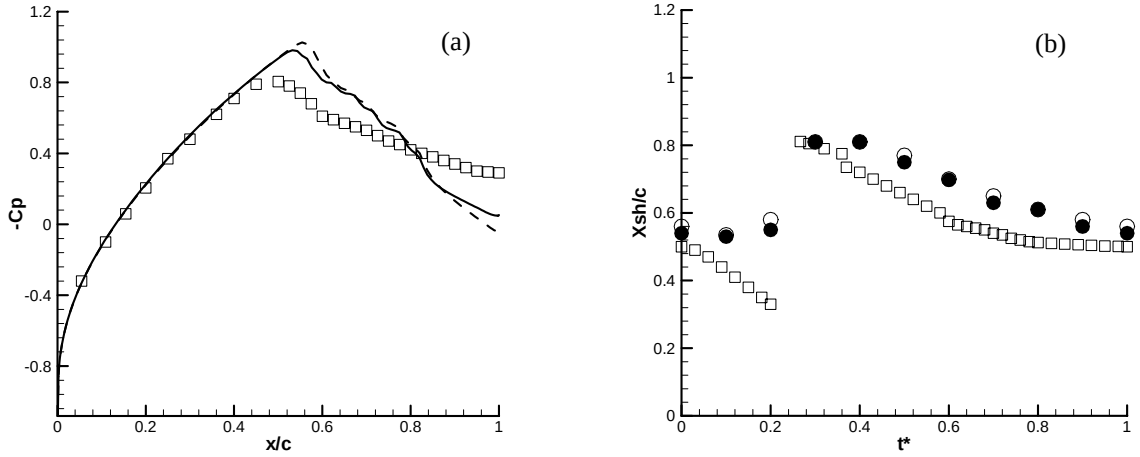

Fig. 7 Time mean pressure coefficient distribution and shock location. (transonic flow around 18% thick circular-arc airfoil $\mathrm{Re}_\infty = 10x10^6, Ma_\infty = 0.76$). (a) Time mean pressure coefficient distribution. Square: experiments, Solid line: with the lag model; Dashed line: without the lag model (b) shock location. Square: experiments; Closed circle: with the lag model; open circle: without the lag model. (t* is shown in Fig. 6(a))

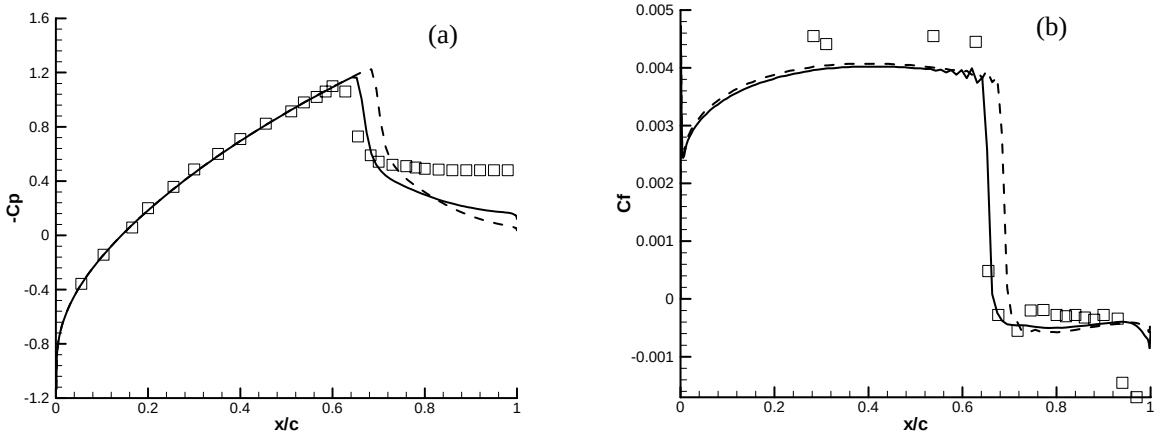

Fig. 8 Pressure coefficient distribution and skin friction distribution. (transonic flow around 18% thick circular-arc airfoil $\mathrm{Re}_\infty = 10x10^6, Ma_\infty = 0.79$) (a) Pressure coefficient distribution. Square: experiments; Solid line: with the lag model; Dashed line: without the lag model. (b) Skin friction coefficient. Square: experiments; Solid line: with the lag model; Dashed line: without the lag model.

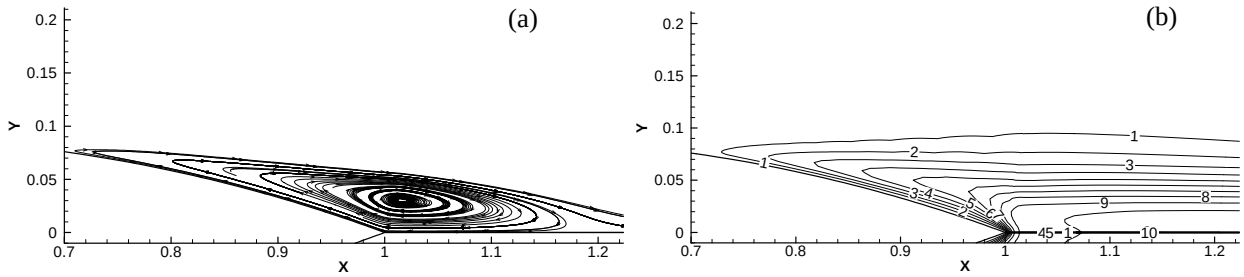

Fig. 9 Streamtrace of velocity vector and turbulent eddy viscosity μ_t contour. (transonic flow around 18% thick circular-arc airfoil $\mathrm{Re}_\infty = 10x10^6, Ma_\infty = 0.79$) (a) Streamtrace (b) turbulent eddy viscosity μ_t contour. With the lag model, maximum value: $\mu_t = 8.15x10^{-4}$, minimum value: $\mu_t = 8.15x10^{-5}$ and interval: $\Delta\mu_t = 8.15x10^{-5}$; without the lag model maximum value: $\mu_t = 2.35x10^{-3}$, minimum value: $\mu_t = 8.15x10^{-5}$ and interval $\mu_t = 2.26x10^{-4}$.

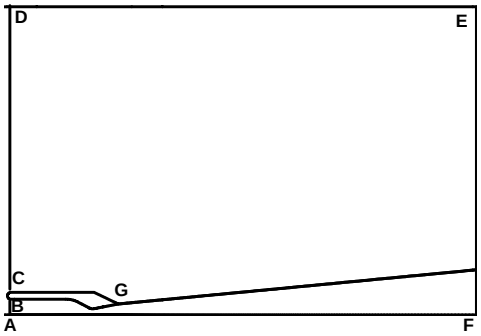

Fig. 10 Computational domain for nozzle flow.

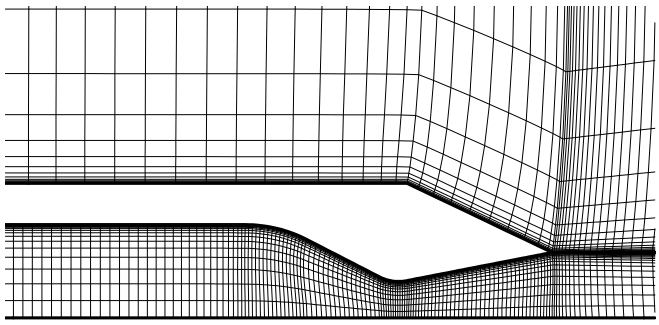

Fig.11 Grid distribution for the nozzle, 1216x128 mesh (For clarity, grid is drawn by skipping 4 grid lines in each directions) .

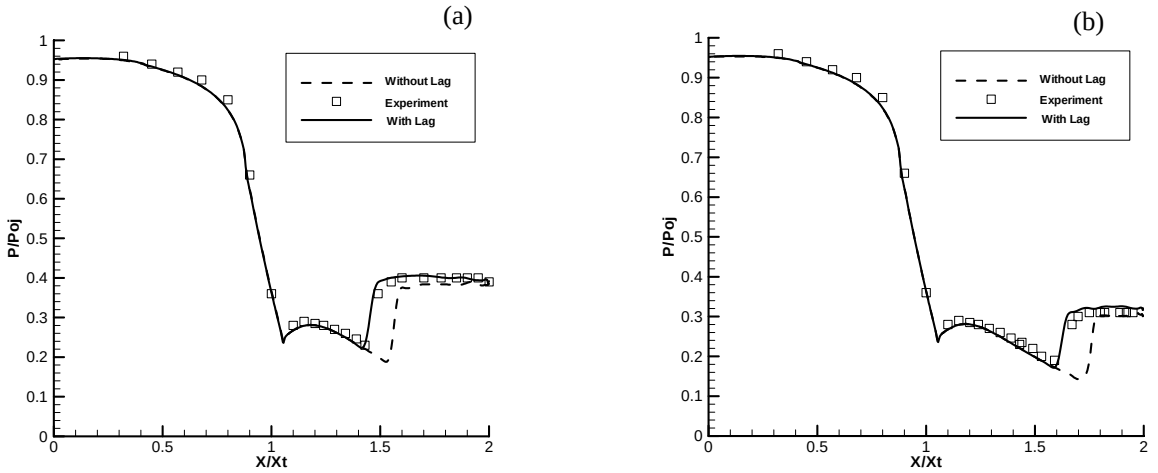

Fig. 12 Top wall pressure distribution for separated nozzle (a) NPR=2.4; (b) NPR=3.0. Square: experiment; Dashed line: without the lag model; Solid line: with the lag model.

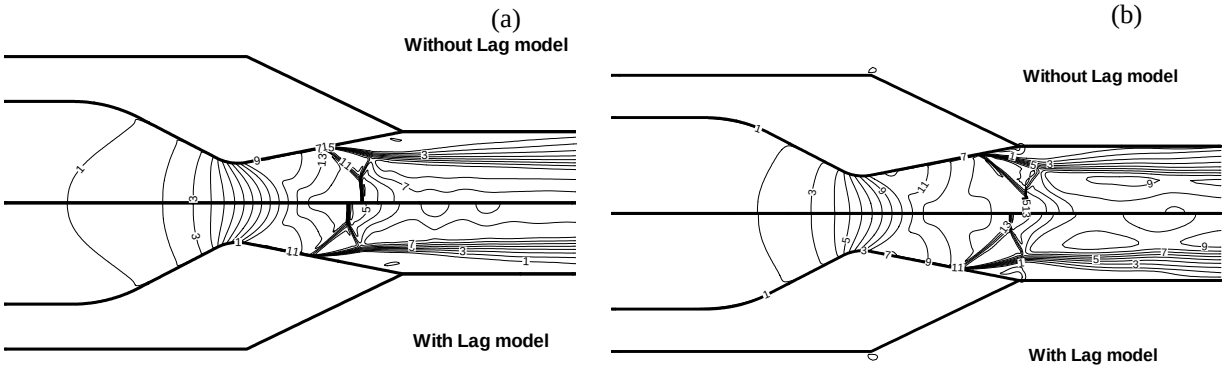

Fig. 13 Mach contour for separated nozzle flow (a) NPR=2.4; maximum value = 1.71, minimum value = 0.24 and interval = 0.24 (b) NPR=3.0 maximum value = 1.91, minimum value = 0.15 and interval = 0.30.

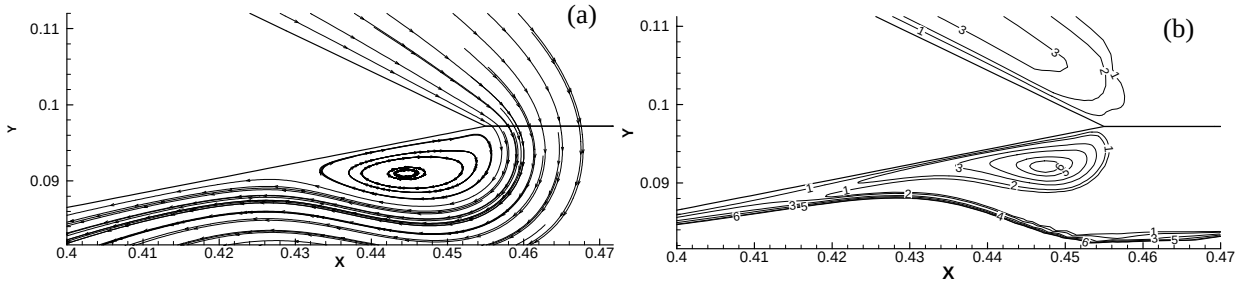

Fig.14 Streamlines and turbulent eddy viscosity contours near the rear part of nozzle for NPR=2.4. (a) Streamlines (b) turbulent eddy viscosity contour. With the lag model maximum value: $\mu_t = 3.47x10^{-5}$; minimum value: $\mu_t = 4.76x10^{-6}$ and interval value: $\Delta\mu_t = 4.99x10^{-6}$; Without the lag model maximum value: $\mu_t = 9.43x10^{-5}$; minimum vale: $\mu_t = 5.42x10^{-6}$ and interval value $\Delta\mu_t = 1.48x10^{-5}$.